RESEARCH ARTICLE

Lubricant hydrogenation over a functionalized clay-based Pd catalyst: A combined computational and experimental study

Zahra Asadi[1] | Samahe Sadjadi[2] | Mehdi Nekoomanesh-Haghighi[1] |
Sergio Posada-Pérez[3] | Miquel Solà[3] | Naeimeh Bahri-Laleh[1] |
Albert Poater[3]

[1]Polymerization Engineering Department, Iran Polymer and Petrochemical Institute (IPPI), Tehran, Iran

[2]Gas Conversion Department, Faculty of Petrochemicals, Iran Polymer and Petrochemical Institute, Tehran, Iran

[3]Institut de Química Computacional i Catàlisi and Departament de Química, Universitat de Girona, Girona, Spain

Correspondence
Samahe Sadjadi, Gas Conversion Department, Faculty of Petrochemicals, Iran Polymer and Petrochemical Institute, PO Box 14975-112. Tehran, Iran.
Email: s.sadjadi@ippi.ac.ir and samahesadjadi@yahoo.com

Naeimeh Bahri-Laleh, Polymerization Engineering Department, Iran Polymer and Petrochemical Institute (IPPI), P.O. Box 14965/115, Tehran, Iran.
Email: n.bahri@ippi.ac.ir

Albert Poater, Institut de Química Computacional i Catàlisi and Departament de Química, Universitat de Girona, c/Maria Aurèlia Capmany 69, 17003 Girona, Catalonia, Spain.
Email: albert.poater@udg.edu

In the world of chemical catalysis and with the importance of being especially in the petrochemical industry, hydrogenation reactions play a central role. Within this framework, the hydrogenation of polyalphaolefins (PAOs) is receiving increasing attention. In this work, for the sake of efficiency and to furnish an efficient support for the immobilization of Pd nanoparticles, a new catalyst containing the 1,3-diaminopropane (DAP) diamine for the decoration of the halloysite (HNT) outer surface is used. The resulting catalytic system exhibited high activity in the hydrogenation of PAOs and high catalyst recyclability since it could be used for several reaction runs, with no appreciable loss of the catalytic activity and Pd leaching. In addition, the nature of the heterogeneous catalysis was demonstrated by a hot filtration test. Density functional theory (DFT) calculations not only unveil the reaction mechanism, in which the rate determining step was determined mechanistically, but also confirm the best location of the palladium nanoparticles, placed between the diamino ligands in the halloysite surface. Furthermore, the computational simulations rationalize why experimentally the catalytic process requires hydrogen pressure of 7 bar and temperature of 130°C to reach high yield.

KEYWORDS
catalyst, halloysite, hydrogenation, Pd nanoparticles, polyalphaolefin

1 | INTRODUCTION

Despite the precision of homogeneous catalysis,[1] heterogeneous catalysis has a much larger impact on our society since most of the important industrial reactions in economic terms, of the present and of the past, are catalyzed by heterogeneous complexes.[2–4] Actually, the pioneering studies in homogeneous catalysis[5] have then the potential to be transformed to heterogenized systems,[6–8] gaining the corresponding efficiency for industry.[9]

The search for cost-effective catalysts by using low-cost and readily available raw materials is challenging.[10–12] In the current search for new catalysts, hydrous aluminum phyllosilicates, that is, clays, have become a family of materials with increasing role in heterogeneous catalysis because they are thermally and chemically stable natural compounds.[13,14]

Clays have the rigidity of heterogeneous catalysts but also the flexibility to allocate frequently several elements inside its structure, including a variety of elements such as iron, as well as alkali metals and alkaline earths. Clay minerals can be distinguished following the general groups classification: kaolin, smectite, illite, chlorite, and a group that joins 2:1 clay type that include palygorskite and sepiolite.[15] During the last decades, the clays have made an almost perfectly symbiotic union with catalysis.[16]

In this context in the family of clays, halloysite nanotube (HNT), which is a dioctahedral 1:1 clay mineral[17–19] of the kaolin family ($Al_2[OH]_4Si_2O_5.nH_2O$), has emerged as a successful material,[20] with origin from volcanic deposits, particularly volcanic ash and glass.[21,22] The unique feature of this clay, that can be found in some countries, such as France, China, and Brazil in large quantity, is its multi-layer tubular morphology.[23] For catalysis, HNTs have layers that are rolled in a way to provide a hollow space,[24,25] specially interesting for catalytic applications. In HNT tubes, the Si–O groups are on the outer surface, while Al–OH groups are on the inner surface.[26–28] These characteristics help to generate tubular micelles.[29,30] On the other hand, both interior and exterior surfaces of HNT are electrically charged and can be modified chemically and electrically.

Chemical modification of HNTs has received considerable attention, and to date, numerous covalent and non-covalent approaches have been disclosed to this purpose[26,31,32] owing to the high thermal and chemical stability of HNTs, as well as its availability and biocompatibility.[33,34] HNTs have an extraordinary ability to be combined with organic ligands,[35,36] or polymers.[37] However, it is necessary to emphasize that the ligands complicate the characterization of the HNT-based systems, since it is even more complex to know the conformation with the metal nanoparticles inserted a posteriori. However, this organic functionalization of HNTs opens up the spectrum of applications in a much broader way,[38–40] and HNTs have the ability to actively participate in those processes.[41–43] However, in homology to chitosan,[44] the participation of a ligand covalently bonded to the HNT was not considered in some works, either by acid treatment to change the diameter of HNT lumen,[45] or changing the HNT hydrophobicity through non-covalent interactions of a surfactant.[40]

Knowing the broad scope of reactions, where HNTs are involved, specifically into the synthesis of organic products,[46] ranging from oxidation reactions[47] to basically hydrogenations,[48] thanks to the high power of molecular hydrogen storage,[49] here we have characterized by experiments and density functional theory (DFT) calculations a HNT-based system, with a diamino ligand capable to trap Pd nanoparticles, in particular, the 1,3-diaminopropane (DAP). The catalytic centers have the catalytic power to hydrogenate polyalphaolefins (PAOs), which is one of the key steps in oil industry,[50,51] if not the most relevant. Such process represents a step forward toward green chemistry and sustainability.[52,53]

2 | EXPERIMENTAL SECTION

2.1 | Reagent

For the synthesis of the catalyst, HNT, (3-chloropropyl) trimethoxysilane (CPTES), 1,3-diaminopropane (DAP), isatoic anhydride (IS), palladium acetate (Pd [OAc]$_2$), sodium borohydride ($NaBH_4 \geq 96\%$), toluene, EtOH, MeOH, and acetonitrile, provided from Sigma-Aldrich (Germany), were used. For the synthesis of PAO, the following list of reagents were used: 1-decene, aluminum chloride ($AlCl_3$) and sodium hydroxide (NaOH >98%), being all purchased from Merck (Germany).

2.2 | Catalyst preparation

2.2.1 | Synthesis of HNT-Cl

First, HNT was reacted with CPTES to provide Cl-functionalized HNT (HNT-Cl) via a nucleophilic substitution reaction, in which the OH functional group in halloysite acts as a nucleophile. Briefly, HNT (3 g) was suspended in toluene (60 ml) and vigorously stirred to furnish a homogeneous suspension. Next, CPTES (2.5 g) were added, and the mixture was refluxed at 110°C under inert (Ar) atmosphere overnight. Upon completion of the process, the precipitate was separated through centrifugation, washed repeatedly with toluene, and dried at 70°C overnight.

2.2.2 | Synthesis of ligand

The ligand used for the functionalization of HNT was prepared according to the previous report.[54] Same as before, the reaction is a nucleophilic substitution, with the difference that in this work the amine takes the role of the nucleophile. Typically, an aqueous solution of DAP (3 mmol in 10-ml deionized water) was prepared and mixed with a solution of IS in EtOH (6 mmol in 40 ml). The resulting mixture was then stirred at 78°C overnight. At the end, the microcrystalline precipitate was separated and purified by recrystallization from EtOH/H_2O, leading to the ligand (L) capable to graft on the HNT.

2.2.3 | Synthesis of HNT-L

To graft the as-synthesized L to HNT-Cl, L (1 g) was added to the suspension of HNT-Cl (2.5 g) in acetonitrile (100 ml) and the mixture was refluxed at 80°C under inert (Ar) atmosphere for 18 h. Afterwards, the precipitate was collected, repeatedly washed with acetonitrile and dried at 50°C overnight.

2.2.4 | Synthesis of Pd/HNT-L

Palladation of HNT-L was performed via the well-established procedure shown in Figure 1,[55] in which Pd NPs interacts with modified HNT-L through electrostatic interactions and/or dative type bonds. Palladation starting from the suspension of HNT-L (2 g) in toluene, and magnetically stirred at the room temperature for 15 min. Separately, Pd (OAc)$_2$ (0.06 g) was dissolved in toluene (5 ml) and slowly added to the stirring suspension of HNT-L. After stirring under Ar atmosphere for 2 h, a fresh solution of $NaBH_4$ (0.2 g in 10 ml MeOH) was prepared and drop-wisely added to HNT-L suspension. Upon introduction of $NaBH_4$ solution, the color of the mixture changed to black, indicating reduction of Pd salt to Pd NPs. Stirring was continued for 2 h at room temperature and then the precipitate was collected, washed with MeOH and dried in oven at 50°C.

2.3 | Synthesis of PAO

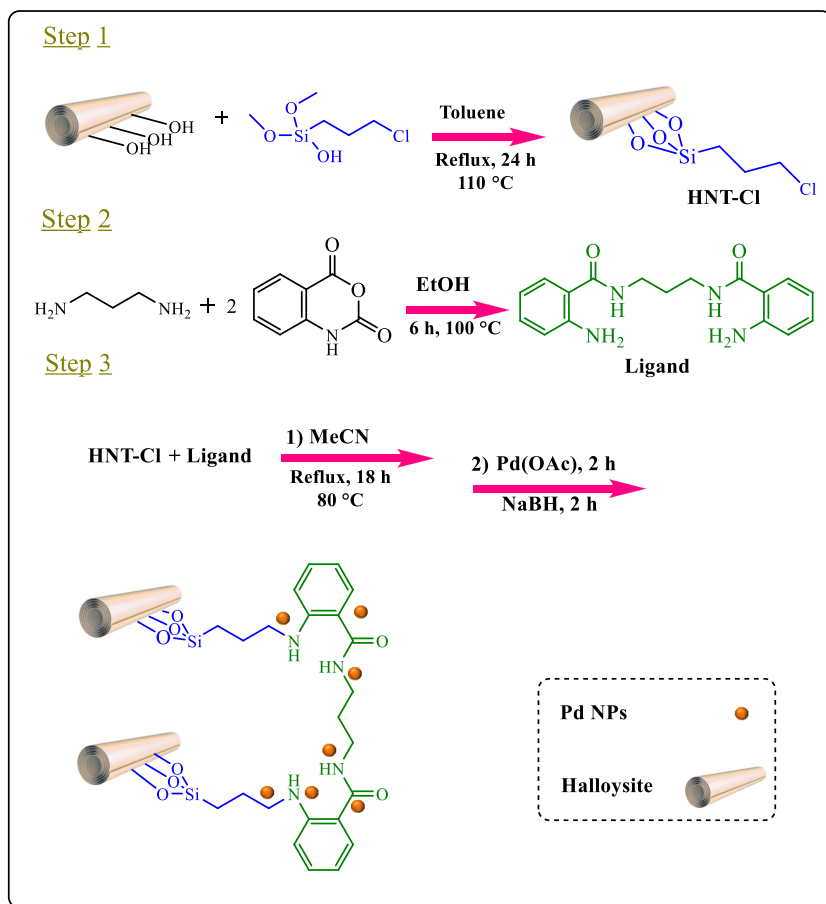The 1-decene oligomerization and synthesis of PAO was fulfilled through the methodology first reported by some

FIGURE 1 Representation of the catalytic synthetic procedure

of us.[50,56,57] In short, the reactor was first prepared by purging N_2 gas for 1 h at 80°C. Then, $AlCl_3$ (5 g) and the mixture of the monomer (500 g) and 0.3-ml deionized water ($H_2O/AlCl_3 = 0.5$ mol/mol) were placed in the reactor. Oligomerization was performed under stirring for 1 h at 100°C. Next the synthesized PAO was collected and washed with NaOH solution (5 wt. %) for several times and then purified by heating under −0.8-bar vacuum up to 250°C. The oligomerization yield achieved was 86%.

2.4 | Hydrogenation of PAO

Hydrogenation of PAO was accomplished according to the previously reported methodology by some of us.[58] Briefly, PAO (10 g) and Pd/HNT-L (5 wt. %) were mixed and placed in a stainless-steel reactor under inert atmosphere. Notably, the air and humidity of the reactor were removed by N_2 purging for 1 h at 100°C. Then, the reactor was sealed, H_2 gas was introduced at a pressure of 7 bar, and the reaction temperature was raised to 130°C. The reaction was continued for 8 h under stirring conditions. Upon completion, the reactor was cooled, and its content was collected. Pd/HNT-L was separated from the as-synthesized PAO via centrifugation, washed with hexane for four times, and dried at 80°C overnight. On the other hand, mention that the yield of hydrogenation of PAO was estimated by ^{1}HNMR spectroscopy.

2.5 | Characterization techniques

2.5.1 | Characterization of Pd/HNT-L

The structural, morphological, and thermal properties of Pd/HNT-L were evaluated using X-ray diffraction (XRD, Siemens, D5000 device with graphite monochromatic Cu-Ka), Fourier transform infrared (FTIR, BRUKER, EQUINOX 55), transmission electron microscopy (TEM, Philips CM30300Kv mod), inductively coupled plasma (ICP-AES, using Vista-pro device), thermogravimetric analysis (TGA, METTLER TOLEDO apparatus, heating rate of 10°C min^{-1} under O_2 atmosphere), energy dispersive spectroscopy (EDS), and elemental mapping analyses (Tescan instrument with acceleration voltage of 20 kV).

2.5.2 | Oil characterization

Nuclear magnetic resonance (^{1}HNMR) spectroscopy was applied for the estimation of the yield of PAO hydrogenation. The used apparatus was Bruker DRX 400 MHz with CDCl$_3$ as solvent at 25°C. The yield of hydrogenation is obtained from the calculation and comparison of the area under peaks of vinylic and allylic hydrogens in the ^{1}HNMR spectra of hydrogenated and unhydrogenated oils according to the following equation:

$$Yield = (1 - A_P/A_T) \times 100$$

where A_P and A_T represent area under the peaks of vinylic and allylic H regions in hydrogenated and unhydrogenated oils, respectively.

2.6 | Computational details

Gaussian 16 package was applied to perform all the DFT calculations.[59] The geometry optimizations were performed using the pure GGA functional of Becke and Perdew, that is, BP86,[60,61] including explicit dispersion corrections to the energy through the Grimme D3 method.[62] In the case of non-metal atoms (i.e., C, H, N, O, Al, and Si) the split-valence basis set (Def2SVP keyword in Gaussian)[63,64] was used, while for Pd the small-core quasi-relativistic Stuttgart/Dresden effective core potential, with an associated valence basis set (standard SDD keyword in Gaussian16) was adopted,[65–67] to address relativistic effects.

The geometry optimizations were carried out without symmetry constraints. Furthermore, even the HNT fragment was also optimized since it is known that it is not rigid. A single Pd atom was used to simulate the Pd content on HNT system.

Analytical frequency calculations were performed to prove the nature of the stationary points, either minima or transition states. In addition, single-point energy calculations using the hybrid GGA functional of Becke-Lee, Parr, and Yang, that is, B3LYP,[68–70] and cc-pVTZ basis set for the non-metal atoms were performed.[71] The reported Gibbs energies in this work include energies obtained at the B3LYP-D3/cc-pVTZ∼SDD//BP86-D3/Def2SVP∼SDD level of theory corrected, with zero-point energies, thermal corrections, and entropy effects evaluated with the BP86-D3/Def2SVP∼SDD method.

3 | RESULTS AND DISCUSSION

### 3.1 | Characterization of Pd/HNT-L

To study the structure and crystallinity of Pd/HNT-L, its XRD pattern was recorded. Furthermore, to appraise whether incorporation of L and immobilization of Pd NPs could affect the structure of HNT, the XRD pattern

of HNT-L and Pd/HNT-L were compared with the HNT XRD. As shown in Figure 2a, XRD patterns of HNT-L and Pd/HNT-L exhibited all of the characteristic peaks of HNT with no shift and displacement (peaks at 2θ = 19.9°, 24.4°, 26.6°, 38.5°, 55.2°, 62.5°, 73.9°, and 77.4°).[28] The only difference was found in the intensity of the peaks in the XRD patterns of HNT-L and Pd/HNT-L, lower than the HNT system, in agreement with past experiments.[45] Noteworthy, the reason for not observing Pd NPs peaks in the XRD pattern of Pd/HNT-L was the formation of fine Pd particles and their homogeneous dispersion on HNT-L.[72]

TG analysis was exploited for studying the thermal stability of Pd/HNT-L. Moreover, the TG curve of the as-prepared catalyst was compared with the bare HNT to approve conjugation of L on HNT. As depicted in Figure 2b, the TG curve of HNT is in good agreement with the literature[28] and shows two weight losses at

120°C and 480°C due to the loss of water and dihydroxylation, respectively. In the case of the TG curve of Pd/HNT-L, a third weight loss can be discerned at 320°C, being indicative of degradation of the organic L. According to the weight loss of this step, the loading of ligand L is estimated as high as 5.37% of the final catalyst weight. In fact, this observation confirms that L has been successfully attached on HNT. Moreover, at high temperature, another weight loss (about 0.8 wt.%) was observed, which can be attributed to the formation of PdO.

To investigate the morphology of Pd/HNT-L and calculate the average of Pd NP size, TEM images of the catalyst were recorded. As it is shown in Figure 3a, HNT tubes can be clearly observed in the TEM image corresponding to Pd/HNT-L catalytic system. This observation established that the tubular morphology of HNT is maintained in the course of chemical modification. Estimation
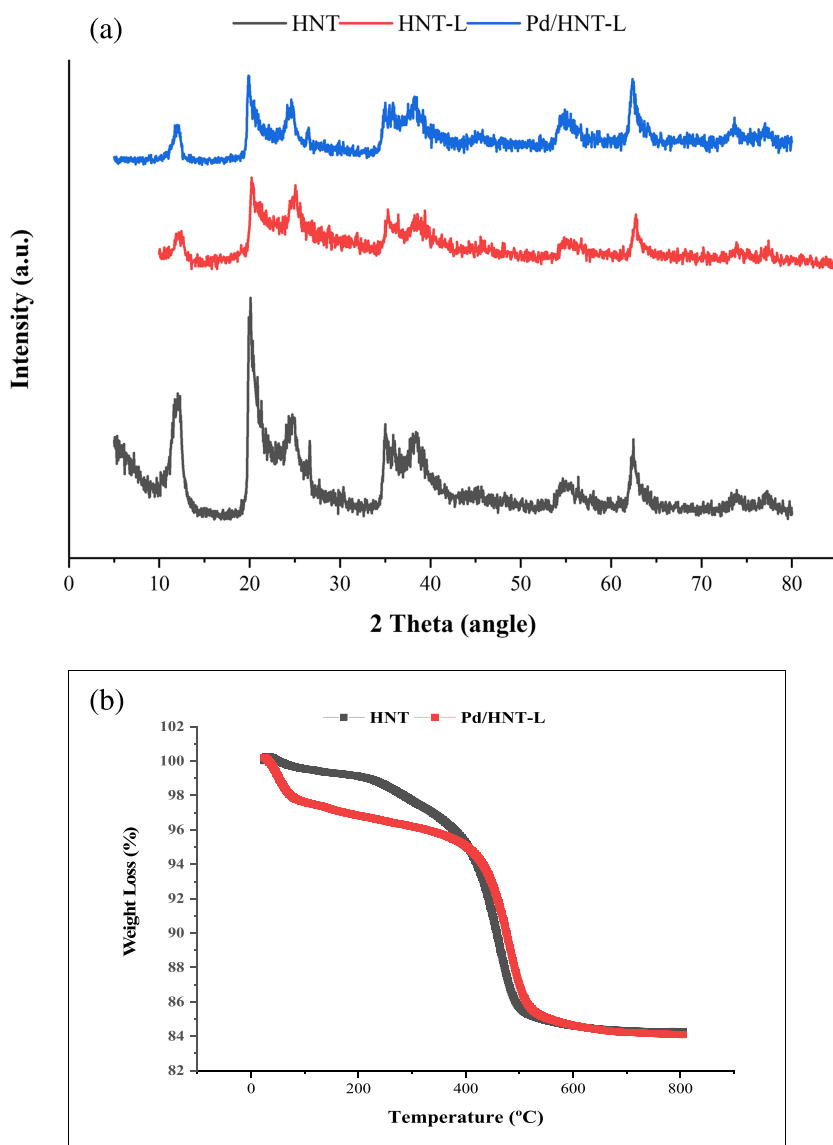
FIGURE 2 (a) X-ray diffraction (XRD) patterns of HNT, HNT-L, and Pd/HNT-L; (b) TG curves of HNT and Pd/HNT-L
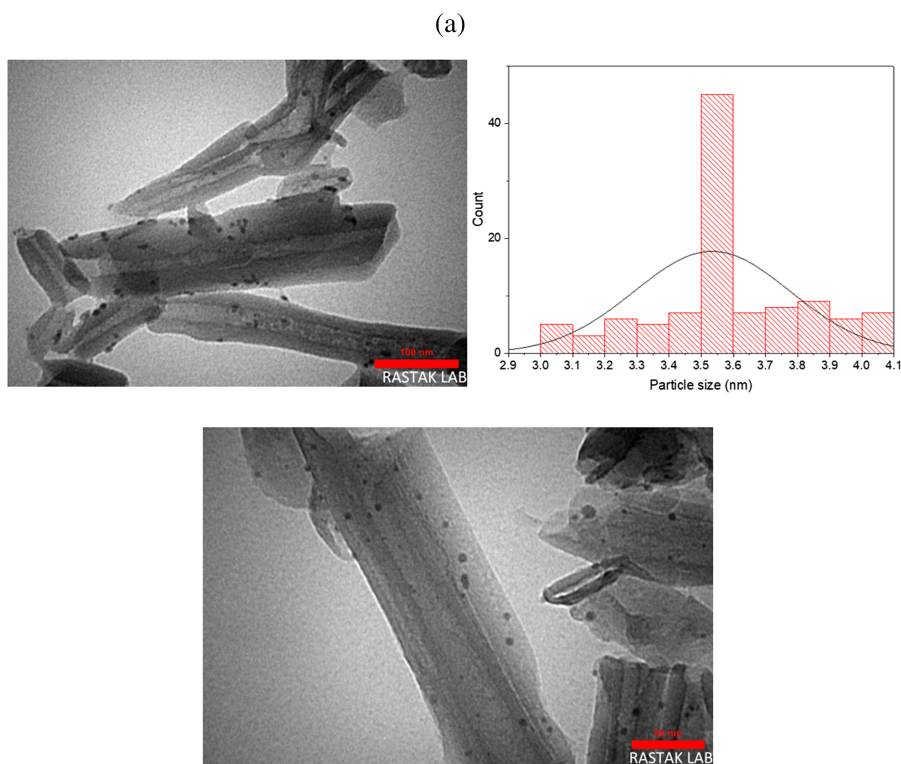
(a)

(b)

of Pd NPs average size indicated formation of fine particles with mean diameter of 3.5 ± 0.2 nm.

In Figure 3b, the elemental mapping analysis of Pd/HNT-L is presented. As it can be observed, the result of this analysis is in good agreement with TEM analysis and approves high dispersion of Pd NPs on HNT-L support. Moreover, homogeneous dispersion of N and C

atoms can indicate the uniform decoration of HNT with the as-prepared L.

With the help of ICP analysis, the loading of Pd NPs in Pd/HNT-L was estimated. This analysis indicated a low Pd content or ~1 wt.%, in the catalyst.

The comparison of FTIR spectrum of Pd/HNT-L and HNT systems is provided in Figure 4. According to the

FIGURE 4 Fourier transform infrared (FTIR) spectra of HNT and Pd/HNT-L
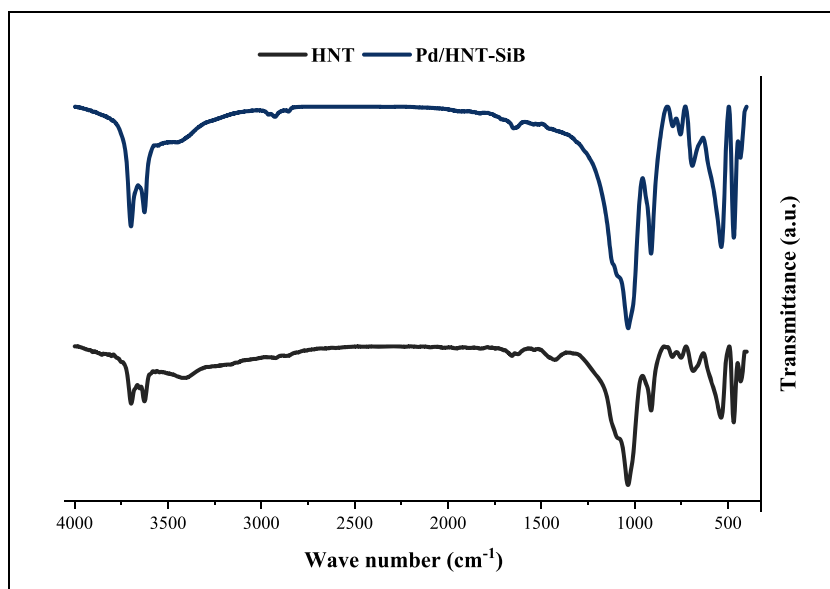
literature,[19] the bands observed in HNT spectrum can be summarized as follows: 536 cm^{-1} (Al-O-Si vibration), 1640 cm^{-1}, 1053 cm^{-1} (Si-O stretching), 3621 cm^{-1}, and 3694 cm^{-1} (inner -OH). The FTIR spectrum of Pd/HNT-L is very similar, containing all of the aforementioned characteristic bands, implying that HNT is structurally stable upon grafting of L. The band observed at 2991 cm^{-1} in the FTIR spectrum of the catalyst is indicative of –CH$_2$ stretching and confirms the grafting of L on HNT. It is worth noting that other characteristic bands of L like the carbonyl band in amide functionality, 1640 cm^{-1}, overlapped with band of Si-O stretching in HNT structure.

3.2 | Hydrogenation of PAO under Pd/HNT-L catalysis

The performance of Pd/HNT-L was examined for the hydrogenation of PAO oil to enhance its characteristic properties.[73,74] Since it was intended to develop a mild and applicable procedure for this process, the factors influencing the reaction were first optimized. The most important variables in this reaction are hydrogen pressure, reaction temperature, and Pd/HNT-L loading. Among this list, hydrogen pressure is the most important from a safety point of view. To optimize the so-called variables, one-variable-at-a-time, OFAT method, was applied, in which the desired parameter is changed, while others are kept constant.

First, the effect of hydrogen pressure was studied. Considering the previous reports on PAO hydrogenation,[75] reaction temperature and Pd/HNT-L loading were kept as 130°C and 5 wt.%, respectively, and the yield of PAO hydrogenation under different hydrogen pressures (6, 7, and 8 bar) was obtained.[76–79] According

to the outcomes in Table 1, hydrogenation yield under hydrogen pressure of 6 bar led to 70%, while increasing the pressure to 7 bar significantly improved the yield of the reaction, reaching a 98% of hydrogenated PAO. This result clearly showed the important effect of hydrogen pressure on the yield of the reaction. Noteworthy, further increase of this parameter to 8 bar did not affect the yield of PAO hydrogenation. Hence, the optimum value for hydrogen pressure was selected as 7 bar.

Next, the effect of the reaction temperature was assayed. These tests, were carried out considering an hydrogen pressure of 7 bar in the presence of 5 wt.% Pd/HNT-L. As summarized in entries 4 and 5 of Table 1, decreasing the reaction temperature to 120°C led to a lower yield of hydrogenated PAO, while increasing the temperature from 130°C to 140°C did not have a substantial effect; hence, the optimum value for this parameter was selected as 130°C. Finally, Pd/HNT-L loading was optimized by measuring the reaction yield in the presence of different loadings of Pd/HNT-L. As listed in entries 6 and 7 of Table 1, this parameter is an influential factor on the yield of PAO hydrogenation; rising the catalyst content from 3 to 5 wt.% led to the increase of the reaction yield from 72% to 98%.

As it is shown in Figure S1, hydrogenation of PAO under the optimized reaction condition ($T = 130$°C, $P = 7$ bar, and 5 wt. % Pd/HNT-L) led to the disappearance of the characteristic peaks of allylic and vinylic hydrogens in the ^{1}HNMR spectrum.

3.3 | Simulation results

The size of metal particles in the supported metal nanostructures is an important factor in determining the

TABLE 1 Study of the effect of hydrogen pressure on the yield of PAO hydrogenation[a]

Entry	H₂ pressure (bar)	Temp. (°C)	Pd/HNT-L loading (wt.%)	PAO hydrogenation yield (%)
1	6	130	5	70
2	7	130	5	98
3	8	130	5	98
4	7	120	5	82
5	7	140	5	98
6	7	130	3	72
7	7	130	4	86

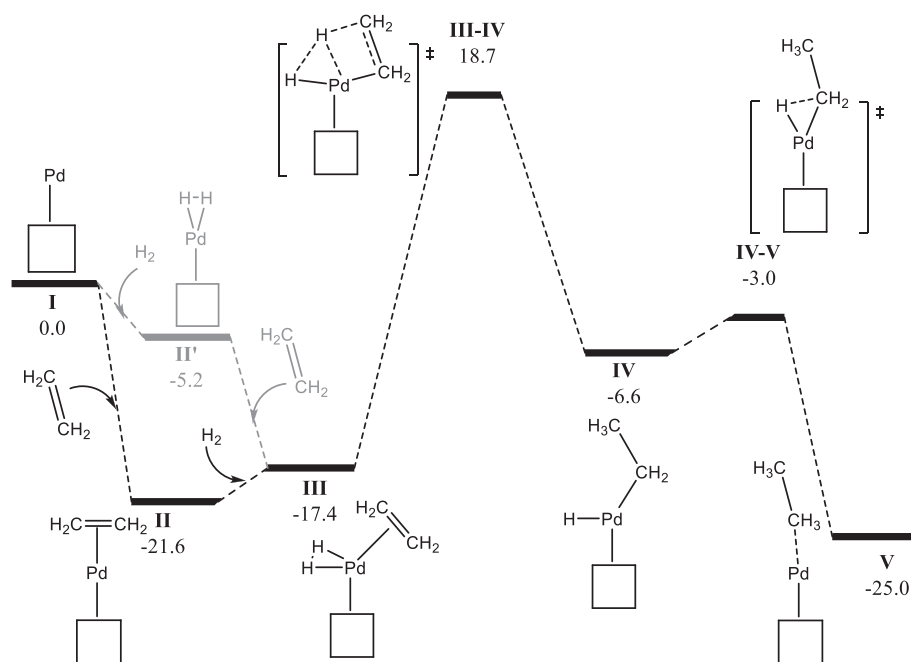[a]Reaction conditions: PAO: 10 g, $T = 130°C$, and 5 wt.% Pd/HNT-L.

FIGURE 5 Computed stationary points for the hydrogenation of ethylene (relative Gibbs energies in kcal/mol, the cube represents the O atoms from the HNT)

performance of heterogeneous catalysts. The single-atom catalyst is accounted as the ultimate small-size limit for metal particles in such catalysts. It contains isolated metal atoms dispersed singly on the employed carriers. This kind of dispersion is crucial for achieving high catalytic activity and selectivity.[80] In the molecular modeling studies utilized in this research an ideal model is employed, which contains single Pd atoms adsorbed on the L decorated HNT, to decrease computational expenses in terms of time and memory. This is a popular technique in the simulation of heterogeneous catalysts and being employed by many authors.[81]

DFT calculations were then used to understand how the palladium metal adsorbed on the L-decorated HNT is capable of reaching close to 100% effectiveness, not at 120°C but at 130°C; and also, because a pressure of 7 bar of H₂ is needed and not less.[82] With a model of the halloysite,[25,43] simply compared to other past studies,[83]

thus, taking ethylene as the model olefin substrate, the hydrogenation mechanism of Figure 5 allows us to see how the palladium with at least one vacancy arranged in intermediate **I** has a greater predisposition to interact with ethylene (intermediate **II**) than with H₂ (intermediate **II'**), thermodynamically by 16.4 kcal/mol. The coordination of both substrates to reach intermediate **III** is not synergistic and implies a relative destabilization of 4.2 kcal/mol owing to the H₂ coordination, being the H-H bond distance 0.897 Å. This already helps to elucidate why 7-bar H₂ pressure is required according to experiments. From this intermediate **III,** the H-transfer from H₂ to the nearest methylene group implies overcoming an energy barrier of 36.1 kcal/mol. Indeed, this barrier has to be calculated from the intermediate **II**, which is lower in energy and then the Gibbs energy barrier increases to 40.3 kcal/mol. This kinetic cost marks the rate determining step (rds) without any discussion,

but it allows us to explain why it is necessary to reach 130°C. Once this first H-transfer has been fulfilled, the second hydrogen migration is carried out from Pd to ethylene, generating the intermediate **IV.** The second hydrogenation process has an energy barrier of only 3.6 kcal/mol, reaching intermediate **V**, with the organic product formed coordinated to Pd atom. The intermediate **V** is the most favored intermediate of the mechanism, 25.3 kcal/mol, with respect to intermediate **I**. Thus, our simulations reveal that thermodynamics (the catalytic cycle is exergonic by 39.3 kcal/mol, here, the formation of ethane from ethylene and molecular hydrogen) is not responsible for the relatively high reaction pressure and temperature determined by experiments. The first hydrogenation step justifies the use of high temperature and pressure to achieve almost perfect conversion.

In terms of characterization, we have compared the first (rds) and second hydrogenation processes. Both transition state structures are displayed in Figure 6a (see

Figures S2–S9 for the rest of intermediates and transition states), where it can be observed that in the TS **IV–V** there are structural factors that explain its relative simplicity. The geometry of the metal center in the latter TS has a perfect square plane geometry, in comparison with the octahedral geometry observed in the TS **III–IV**. Moreover, in the latter case the three oxygen atoms bonded to palladium that report electron density and the metal suffer considerable distortion, being placed in a non-meridional, but facial conformation. In addition, to confirm quantitatively these statements, the $\%V_{Bur}$ and steric maps of Cavallo and coworkers confirm that the metal center pushes toward a more facile H-transfer for TS **IV–V** than for TS **III–IV**.

Unlike other movements in transition states, here the distance from hydrogen to the target carbon of the alkene must be as small as possible, and therefore, steric pressure through the ligands would favor it. To validate qualitatively and quantitatively account this hypothesis, steric

(a)

(b)
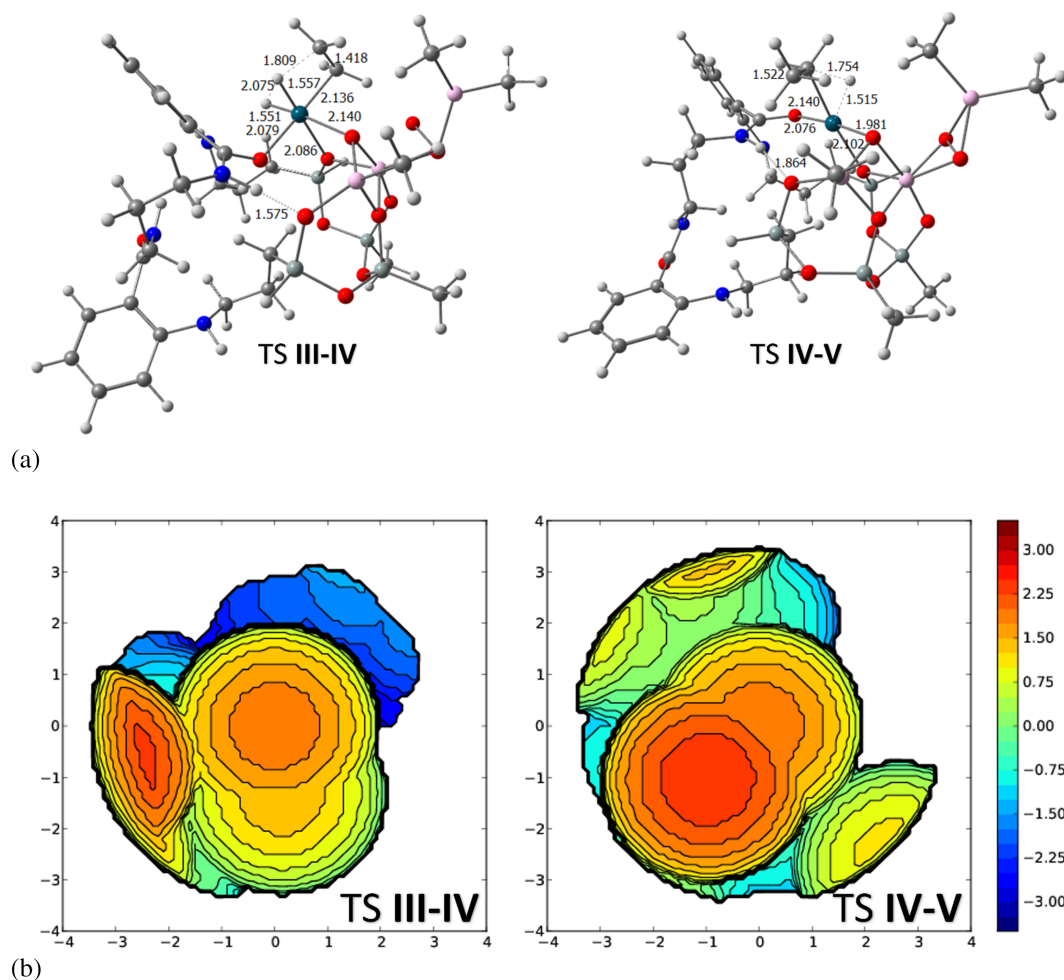
FIGURE 6 (a) Optimized structures at the BP86-D3/Def2SVP∼SDD level of theory of the computed TS **III–IV** (left) and TS **IV–V** (right), selected distances in Å. (b) Steric maps of TS **III–IV** (left) and TS **IV–V** (right); xy plane, with the carbon atom that receives the H-transfer in the center and the z axis crossing the palladium, and the H that is transferred part of the xz plane; curves are given in Å.

maps and the buried volume, $\%V_{Bur}$, of the designed catalysts were computed using the SambVca2.1 package.[84,85] Turning to the results, the $\%V_{Bur}$ is 60.9% for TS **IV–V** and only 50.4% for TS **III–IV**. This is a significant change, and furthermore, if going to the analysis of the two quadrants where the H-transfer occurs, the values are 38.2% and 33.1% for TS **III–IV**, while 58.5% and 36.4% for TS **IV–V**. Therefore, in the second H-transfer the steric pressure greatly facilitates the process, as the steric maps in Figure 6b graphically confirm (see Figures S10 and S11 for further details).

Regarding previous studies, the ligand with three methylene units between the two NH groups does not directly bond to the palladium center, but it causes a strong stabilization since NH group forms a strong H-bond with a halloysite oxygen. Thus, indirectly, this fact causes that the palladium, which would presumably simply settle around the nitrogen atoms, migrates to an environment of up to three oxygen atoms, including the keto group that links the HNT with the diamino ligand. Any 3D view of the computed species (see Supporting Information) helps to understand how this NH···O interaction is simply key, and it moves with values of 2.003, 1.869, 1.816, 1.959, and 1.864 Å for the intermediates **I** to **V**, respectively. This interaction, in principle expected to be weak, is so strong that reaches Mayer Bond Orders (MBO)[86] up to 0.222 in TS **III–IV**, for example.

3.4 | Catalyst recyclability

Catalysts with high recyclability are of great demand due to their potential for industrial uses. To assay whether Pd/HNT-L can be reused efficiently, classic recyclability test was accomplished. As mentioned in Section 2, the recovered Pd/HNT-L was washed with hexane, dried, and reused for the next run of PAO hydrogenation. As presented in Figure 7a, reuse of Pd/HNT-L for the second run led to negligible loss of the catalytic activity (only 2%). Further reuse of Pd/HNT-L up to fifth run was also carried out, and the results indicated slight loss of activity upon each recycling, showing that Pd/HNT-L is a recyclable catalyst.

According to previous results,[28] the loss of the catalyst's activity can be ascribed to the leaching of the palladium NPs, i.e., the main catalytic component. To measure the Pd leaching, the loading of Pd on the recovered catalyst after fifth run was measured via ICP and compared with the fresh one. Gratifyingly, even after five runs of the hydrogenation reaction, Pd leaching was insignificant (only 0.8 wt.% of initial loading).

It is worth mentioning that there are three groups of mechanisms responsible for the deactivation of a heterogeneous catalyst: chemical, mechanical, and thermal. Chemical deactivation comprises poisoning; leaching or vapor compound formation and solid–solid and/or vapor–solid reactions while mechanical deactivation includes attrition/crushing.[87] In our case, although the catalyst leaching was negligible, other mechanisms would occur which caused catalyst activity decay after five runs of hydrogenation experiments. In fact, it is also possible that deposition of PAO on the surface of the catalyst could deactivate some of the catalytic active sites.

3.5 | Hot filtration

The nature of the catalysis was appraised via hot-filtration method. In this regard, PAO hydrogenation under the optimum reaction condition, $P = 7$ bar and $T = 130°$C, was conducted for 1 h, and then the hydrogenation was stopped and Pd/HNT-L was removed from the reactor via centrifugation. Subsequently, the reactor was sealed again, and the reaction was continued in the
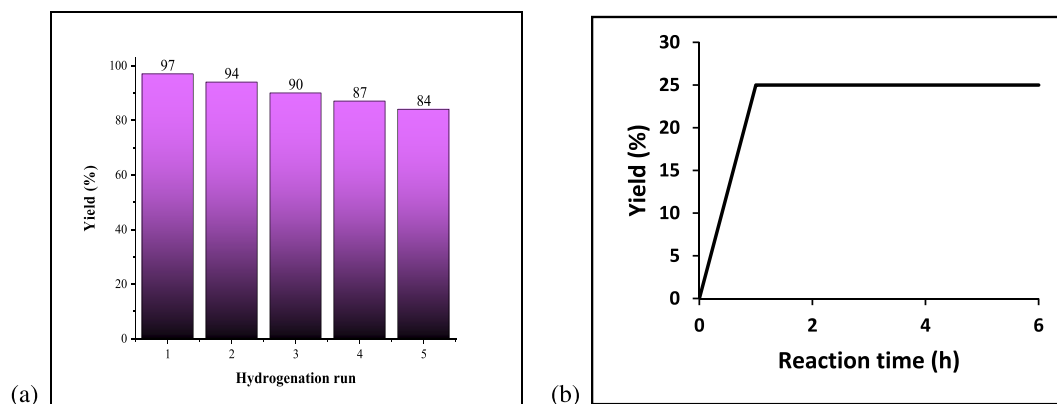

(a)   (b)

FIGURE 7 (a) The recycling results of Pd/HNT-L for PAO hydrogenation. (b) The results of hot-filtration test for PAO hydrogenation under optimum reaction condition

absence of Pd/HNT-L. In Figure 7b the yield of the reaction was monitored for 6 h and the yield of PAO hydrogenation was estimated. The results clearly demonstrated that the reaction did not proceed in the absence of Pd/HNT-L, approving the fact that Pd NPs were not leached in the course of hydrogenation and catalysis was heterogeneous in nature.

4 | CONCLUSIONS

A Pd/HNT-L catalytic system was synthesized and used as a heterogeneous catalyst to investigate the hydrogenation of PAOs, combining experimental and theoretical studies, for the right characterization of the metal center and mechanistic insights. Experimental studies revealed that the best performance for the hydrogenation process is obtained not at mild conditions, but at relatively high temperature (130°C) and pressure (7 bar), making a thermodynamic surgery almost, since neither at 120°C nor at 6 bar the performance was so remarkable. Simulations revealed that Pd is eager to be coordinated with ethylene than with H_2, which suggests the need of relatively high pressure of the gas to facilitate the formation of the intermediate that coordinate H_2 and ethylene all together. In addition, the energy profile was computed, showing a very large energy barrier for the first semihydrogenation of the C-C bond (40.3 kcal/mol), which is the rds of the reaction, and providing an explanation about the need for harsh reaction conditions. Notably, Pd/HNT-L showed good recyclability and only slight loss of catalytic activity and Pd leaching were detected upon each run of recycling.

AUTHOR CONTRIBUTIONS
Zahra Asadi: Formal analysis; investigation; visualization; data curation. **Samahe Sadjadi:** Data curation; formal analysis; methodology; supervision; validation; conceptualization. **Mehdi Nekoomanesh-Haghighi:** Project administration; validation; conceptualization; formal analysis; funding acquisition. **Sergio Posada-Pérez:** Data curation; formal analysis; investigation; validation; visualization. **Miquel Solà:** Formal analysis; supervision; validation; funding acquisition; conceptualization. **Naeimeh Bahri-Laleh:** Conceptualization; data curation; formal analysis; funding acquisition; methodology; supervision; investigation. **Albert Poater:** Conceptualization; data curation; formal analysis; funding acquisition; investigation; supervision; validation; visualization.

CONFLICT OF INTEREST
There is no conflict to declare.

DATA AVAILABILITY STATEMENT
The data that support the findings of this study are available in the supporting information of this article. *Xyz* coordinates and absolute energies of all computed species are included in Table S1.

ORCID
Zahra Asadi https://orcid.org/0000-0002-4123-7421
Samahe Sadjadi https://orcid.org/0000-0002-6884-4328
Mehdi Nekoomanesh-Haghighi https://orcid.org/0000-0002-6997-6787
Sergio Posada-Pérez https://orcid.org/0000-0003-4200-4264
Miquel Solà https://orcid.org/0000-0002-1917-7450
Naeimeh Bahri-Laleh https://orcid.org/0000-0002-0925-5363
Albert Poater https://orcid.org/0000-0002-8997-2599

REFERENCES
[1] F. Zaera, *Chem. Rev.* **2022**, *122*, 8594.
[2] G. J. Hutchings, *Faraday Discuss.* **2021**, *229*, 9.
[3] N. Bahri-Laleh, A. Hanifpour, S. A. Mirmohammadi, A. Poater, M. Nekoomanesh-Haghighi, G. Talarico, L. Cavallo, *Prog. Polym. Sci.* **2018**, *84*, 89.
[4] M. Fallah, N. Bahri-Laleh, K. Didehban, A. Poater, *Appl. Organomet. Chem.* **2020**, *34*, e5333.
[5] V. D'Elia, H. Dong, A. Rossini, C. Widdifield, S. V. C. Vummaleti, Y. Minenkov, A. Poater, E. Abou-Hamad, J. D. A. Pelletier, L. Cavallo, L. Emsley, J. M. Basset, *J. Am. Chem. Soc.* **2015**, *137*, 7728.
[6] S. Zhang, Q. Fan, R. Xia, T. J. Meyer, *Acc. Chem. Res.* **2020**, *53*, 255.
[7] V. D'Elia, A. A. Ghani, A. Monassier, J. Sofack-Kreutzer, J. D. A. Pelletier, M. Drees, S. V. C. Vummaleti, A. Poater, L. Cavallo, M. Cokoja, J.-M. Basset, F. E. Kühn, *Chem. – Eur. J.* **2014**, *20*, 11870.
[8] S. K. Kaiser, Z. Chen, D. Faust Akl, S. Mitchell, J. Pérez-Ramírez, *Chem. Rev.* **2020**, *120*, 11703.
[9] C. M. Hendrich, K. Sekine, T. Koshikawa, K. Tanaka, A. S. K. Hashmi, *Chem. Rev.* **2021**, *121*, 9113.
[10] N. Mizuno, M. Misono, *Chem. Rev.* **1998**, *98*, 199.
[11] F. Zaera, *Coord. Chem. Rev.* **2021**, *448*, 214179.
[12] S. E. S. Leonhardt, A. Stolle, B. Ondruschka, G. Cravotto, C. D. Leo, K. D. Jandt, T. F. Keller, *Appl. Catal. A* **2010**, *379*, 30.

[13] Z. Li, Y. Sun, Y. Yang, Y. Han, T. Wang, J. Chen, D. C. W. Tsang, *Environ. Res.* **2020**, *183*, 109156.

[14] J. Amaya, L. Bobadilla, L. Azancot, M. Centeno, S. Moreno, R. Molina, *Mater. Res. Bull.* **2020**, *123*, 110728.

[15] H. H. Murray, *Appl. Clay Sci.* **2000**, *17*, 207.

[16] A. Vaccari, *Appl. Clay Sci.* **1999**, *14*, 161.

[17] Z. Li, L. Liu, A. Jiménez González, D.-Y. Wang, *Polym. Chem.* **2017**, *8*, 3926.

[18] P. Yuan, D. Tan, F. Annabi-Bergaya, *Appl. Clay Sci.* **2015**, *112-113*, 75.

[19] L. Lisuzzo, G. Cavallaro, S. Milioto, G. Lazzara, *J. Colloid Interface Sci.* **2022**, *608*, 424.

[20] J. Hamdi, B. N. Diehl, K. Kilgore, S. A. Lomenzo, M. L. Trudell, *ACS Omega* **2019**, *4*, 19437.

[21] J. Ouyang, D. Mu, Y. Zhang, H. Yang, *Minerals* **2018**, *8*, 108.

[22] J. Ouyang, T. Liu, H. Yang, Y. Zhang, *J. Colloid Interface Sci.* **2019**, *555*, 509.

[23] Y. Fu, L. Zhang, *J. Solid State Chem.* **2005**, *178*, 3595.

[24] D. Papoulis, *Appl. Clay Sci.* **2019**, *168*, 164.

[25] N. Bahri-Laleh, S. Sadjadi, M. M. Heravi, M. Malmir, *Appl. Organomet. Chem.* **2018**, *32*, e4283.

[26] M. Massaro, C. G. Colletti, G. Lazzara, S. Milioto, R. Noto, S. Riela, *J. Mater. Chem. A* **2017**, *5*, 13276.

[27] J. Zare Pirhaji, F. Moeinpour, A. Mirhoseini Dehabadi, S. A. Yasini Ardakani, *Appl. Organomet. Chem.* **2020**, *34*, e5640.

[28] S. Sadjadi, *Appl. Clay Sci.* **2020**, *189*, 105537.

[29] G. Lazzara, G. Cavallaro, A. Panchal, R. Fakhrullin, A. Stavitskaya, V. Vinokurov, Y. Lvov, *Curr. Opin. Colloid Interface Sci.* **2018**, *35*, 42.

[30] G. Cavallaro, G. Lazzara, S. Milioto, F. Parisi, *Langmuir* **2015**, *31*, 7472.

[31] M. Massaro, G. Lazzara, S. Milioto, R. Noto, S. Riela, *J. Mater. Chem. B* **2017**, *5*, 2867.

[32] J. Ouyang, B. Guo, L. Fu, H. Yang, Y. Hu, A. Tang, H. Long, Y. Jin, J. Chen, J. Jiang, *Mater. Des.* **2016**, *110*, 169.

[33] N. Danyliuk, J. Tomaszewska, T. Tatarchuk, *J. Mol. Liq.* **2020**, *309*, 113077.

[34] L. Lisuzzo, G. Cavallaro, S. Milioto, G. Lazzara, *Appl. Clay Sci.* **2020**, *185*, 105416.

[35] S. Sadjadi, M. M. Heravi, M. Malmir, F. G. Kahangi, *Appl. Clay Sci.* **2018**, *162*, 192.

[36] Z. Chen, D. Mu, T. Liu, Z. He, Y. Zhang, H. Yang, J. Ouyang, *J. Colloid Interface Sci.* **2021**, *582*, 137.

[37] S. Sadjadi, M. Akbari, E. Monflier, M. M. Heravi, B. Leger, *New J. Chem.* **2018**, *42*, 15733.

[38] E. Rafiee, M. Kahrizi, *J. Mol. Liq.* **2016**, *218*, 625.

[39] R. Teimuri-Mofrad, M. Gholamhosseini-Nazari, E. Payami, S. Esmati, *Appl. Organomet. Chem.* **2018**, *32*, e3955.

[40] A. Shams, S. Sadjadi, J. Duran, S. Simon, A. Poater, N. Bahri-Laleh, *Appl. Organomet. Chem* **2022**, e6719.

[41] S. Sadjadi, M. Akbari, M. M. Heravi, *ACS Omega* **2019**, *4*, 19442.

[42] M. Mehdizadeh, S. Sadjadi, A. Poater, A. Mansouri, N. Bahri-Laleh, *J. Mol. Liq.* **2022**, *352*, 118675.

[43] S. Sadjadi, F. Koohestani, G. Pareras, M. Nekoomanesh-Haghighi, N. Bahri-Laleh, A. Poater, *J. Mol. Liq.* **2021**, *331*, 115740.

[44] M. Alleshagh, S. Sadjadi, H. Arabi, N. Bahri-Laleh, E. Monflier, *J. Phys. Chem. Solids* **2022**, *164*, 110611.

[45] Z. Asadi, S. Sadjadi, M. Nekoomanesh-Haghighi, N. Bahri-Laleh, *Inorg. Chem. Commun.* **2022**, *140*, 109438.

[46] A. Mahajan, P. Gupta, *New J. Chem.* **2020**, *44*, 12897.

[47] M. J. Baruah, T. J. Bora, R. Dutta, S. Roy, A. K. Guha, K. K. Bania, *Mol. Catal.* **2021**, *515*, 111858.

[48] Z. Zhu, D. Ding, Y. Zhang, Y. Zhang, *Appl. Clay Sci.* **2020**, *196*, 105761.

[49] J. Jin, J. Ouyang, H. Yang, *Nanoscale Res. Lett.* **2017**, *12*, 240.

[50] S. Karimi, N. Bahri-Laleh, G. Pareras, S. Sadjadi, M. Nekoomanesh-Haghighi, A. Poater, *J. Ind. Eng. Chem.* **2021**, *97*, 441.

[51] S. Gharajedaghi, Z. Mohamadnia, E. Ahmadi, M. Marefat, G. Pareras, S. Simon, A. Poater, N. Bahri-Laleh, *Mol. Catal.* **2021**, *509*, 111636.

[52] J. H. Clark, R. Luque, A. S. Matharu, *Annu. Rev. Chem. Biomol. Eng.* **2012**, *3*, 183.

[53] A. Hanifpour, N. Bahri-Laleh, M. Nekoomanesh-Haghighi, A. Poater, *Green Chem.* **2022**, *22*, 4617.

[54] J. Safaei-Ghomi, R. Teymuri, *Appl. Organomet. Chem.* **2019**, *33*, e5150.

[55] S. Sadjadi, M. Akbari, B. Léger, E. Monflier, M. M. Heravi, *ACS Sustainable Chem. Eng.* **2019**, *7*, 6720.

[56] A. Hanifpour, N. Bahri-Laleh, M. Nekoomanesh-Haghighi, A. Poater, *Appl. Organomet. Chem.* **2021**, *34*, e6227.

[57] A. Hanifpour, N. Bahri-Laleh, M. Nekoomanesh-Haghighi, A. Poater, *Mol. Catal.* **2020**, *493*, 111047.

[58] M. Tabrizi, S. Sadjadi, G. Pareras, M. Nekoomanesh-Haghighi, N. Bahri-Laleh, A. Poater, *J. Colloid Interface Sci.* **2021**, *581*, 939.

[59] Gaussian 16, Revision C.01, M. J. Frisch, G. W. Trucks, H. B. Schlegel, G. E. Scuseria, M. A. Robb, J. R. Cheeseman, G. Scalmani, V. Barone, G. A. Petersson, H. Nakatsuji, X. Li, M. Caricato, A. V. Marenich, J. Bloino, B. G. Janesko, R. Gomperts, B. Mennucci, H. P. Hratchian, J. V. Ortiz, A. F. Izmaylov, J. L. Sonnenberg, D. Williams-Young, F. Ding, F. Lipparini, F. Egidi, J. Goings, B. Peng, A. Petrone, T. Henderson, D. Ranasinghe, V. G. Zakrzewski, J. Gao, N. Rega, G. Zheng, W. Liang, M. Hada, M. Ehara, K. Toyota, R. Fukuda, J. Hasegawa, M. Ishida, T. Nakajima, Y. Honda, O. Kitao, H. Nakai, T. Vreven, K. Throssell, J. A. Montgomery, Jr., J. E. Peralta, F. Ogliaro, M. J. Bearpark, J. J. Heyd, E. N. Brothers, K. N. Kudin, V. N. Staroverov, T. A. Keith, R. Kobayashi, J. Normand, K. Raghavachari, A. P. Rendell, J. C. Burant, S. S. Iyengar, J. Tomasi, M. Cossi, J. M. Millam, M. Klene, C. Adamo, R. Cammi, J. W. Ochterski, R. L. Martin, K. Morokuma, O. Farkas, J. B. Foresman, and D. J. Fox, Gaussian, Inc., Wallingford CT, **2016**.

[60] A. D. Becke, *Phys. Rev. A* **1988**, *38*, 3098.

[61] J. P. Perdew, *Phys. Rev. B* **1986**, *33*, 8822.

[62] S. Grimme, J. Antony, S. Ehrlich, H. Krieg, *J. Chem. Phys.* **2010**, *132*, 154104.

[63] F. Weigend, R. Ahlrichs, *Phys. Chem. Chem. Phys.* **2005**, *7*, 3297.

[64] F. Weigend, *Phys. Chem. Chem. Phys.* **2006**, *8*, 1057.

[65] U. Häussermann, M. Dolg, H. Stoll, H. Preuss, P. Schwerdtfeger, R. Pitzer, *Mol. Phys.* **1993**, *78*, 1211.

[66] W. Küchle, M. Dolg, H. Stoll, H. Preuss, *J. Chem. Phys.* **1994**, *100*, 7535.

[67] T. Leininger, A. Nicklass, H. Stoll, M. Dolg, P. Schwerdtfeger, *J. Chem. Phys.* **1996**, *105*, 1052.

[68] A. D. Becke, *J. Chem. Phys.* **1993**, *98*, 5648.

[69] C. Lee, W. Yang, R. G. Parr, *Phys. Rev. B* **1988**, *37*, 785.

[70] P. J. Stephens, F. J. Devlin, C. F. Chabalowski, M. J. Frisch, *J. Phys. Chem.* **1994**, *98*, 11623.

[71] T. H. Dunning Jr., *J. Chem. Phys.* **1989**, *90*, 1007.

[72] S. Mallik, S. S. Dash, K. M. Parida, B. K. Mohapatra, *J. Colloid Interface Sci.* **2006**, *300*, 237.

[73] A. Hanifpour, N. Bahri-Laleh, A. Mohebbi, M. Nekoomanesh-Haghighi, *Iran. Polym. J.* **2022**, *31*, 107.

[74] T. Ritter, H. Alt, *Polyolefins J.* **2020**, *7*, 79.

[75] M. Alleshagh, S. Sadjadi, H. Arabi, N. Bahri-Laleh, E. Monflier, *Mater. Chem. Phys.* **2021**, *278*, 125506.

[76] V. V. Nedolivko, G. O. Zasypalov, Y. A. Chudakov, A. V. Vutolkina, A. A. Pimerzin, A. P. Glotov, *Russ. Chem. Bull.* **2020**, *69*, 260.

[77] A. Glotov, A. Vutolkina, A. Pimerzin, V. Vinokurov, Y. Lvov, *Chem. Soc. Rev.* **2021**, *50*, 9240.

[78] A. Glotov, A. Novikov, A. Stavitskaya, V. Nedolivko, D. Kopitsyn, A. Kuchierskaya, E. Ivanov, V. Stytsenko, V. Vinokurov, Y. Lvov, *Catal. Today* **2021**, *378*, 33.

[79] A. Glotov, A. Vutolkina, A. Pimerzin, V. Nedolivko, G. Zasypalov, V. Stytsenko, E. Karakhanov, V. Vinokurov, *Catalysts* **2020**, *10*, 537.

[80] X.-F. Yang, A. Wang, B. Qiao, J. Li, J. Liu, T. Zhang, *Acc. Chem. Res.* **2013**, *46*, 1740.

[81] D. Astruc, G. Bertrand, M. Eddaoudi, Y. Han, K.-W. Huang, J. Lercher, C. Santini, K. Takanabe, M. Taoufik, L. Cavallo, *ACS Catal.* **2022**, *12*, 4961.

[82] S. Dehghani, S. Sadjadi, N. Bahri-Laleh, M. Nekoomanesh-Haghighi, A. Poater, *Appl. Organomet. Chem.* **2019**, *33*, e4891.

[83] F. Ferrante, N. Armata, G. Lazzara, *J. Phys. Chem. C* **2015**, *119*, 16700.

[84] L. Falivene, R. Credendino, A. Poater, A. Petta, L. Serra, R. Oliva, V. Scarano, L. Cavallo, *Organometallics* **2016**, *35*, 2286.

[85] L. Falivene, Z. Cao, A. Petta, L. Serra, A. Poater, R. Oliva, V. Scarano, L. Cavallo, *Nat. Chem.* **2019**, *11*, 872.

[86] I. Mayer, *Chem. Phys. Lett.* **1983**, *97*, 270.

[87] M. D. Argyle, C. H. Bartholomew, *Catalysts* **2014**, *5*, 145.

SUPPORTING INFORMATION

Additional supporting information can be found online in the Supporting Information section at the end of this article.